ACS Catalysis

pubs.acs.org/acscatalysis

Research Article

Inhibiting the Hydrogen Evolution Reaction (HER) with Proximal Cations: A Strategy for Promoting Selective Electrocatalytic Reduction

Jeffrey M. Barlow, Joseph W. Ziller, and Jenny Y. Yang*

Cite This: *ACS Catal.* 2021, 11, 8155–8164

Read Online

ACCESS | Metrics & More | Article Recommendations | Supporting Information

ABSTRACT: Most electrochemical reduction reactions require protons; however, direct reduction of protons to hydrogen is a common competitive side reaction that lowers the overall yield (Faradaic efficiency) for the desired product. Inhibition of the hydrogen evolution reaction (HER) by fixed, proximal mono- or dication is reported. An SNS tridentate ligand with a pendant aza-crown functionality and the corresponding Pd(II) and Rh(I) complexes were synthesized. For the Pd complexes, the presence of a Na^+ or Ba^{2+} ion in the aza-crown increases the overpotential for hydrogen evolution by up to 260 mV compared to a congener that lacks an aza-crown. The increase in the overpotential for HER was observed with cationic and neutral acids in both acetonitrile and dimethylformamide. Additionally, for the Pd complexes, the inclusion of a Ba^{2+} ion into the aza-crown modestly improved the selectivity for electrocatalytic CO_2 reduction to CO, whereas H_2 was the only product for the congener lacking the aza-crown. The Ba^{2+}-containing complex also had improved catalytic stability, although all complexes were ultimately unstable under prolonged electrolytic conditions. The increase in the overpotential for HER through the installation of a local charge exemplifies an effective catalyst design strategy for inhibiting the hydrogen evolution reaction.

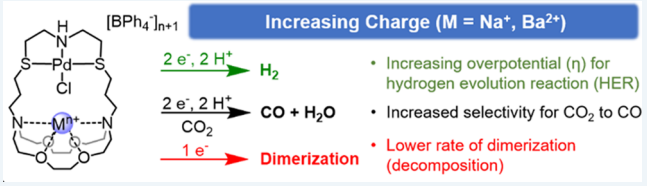

KEYWORDS: *hydrogen evolution reaction, selective electrocatalytic reduction, Faradaic efficiency, proximal cation, CO_2 reduction reaction*

There is increasing enthusiasm for the use of electrochemical methods in synthesis and catalysis, with applications ranging from organic transformations[1−8] to the generation of fuels from feedstocks.[10−14] Electrosynthesis and electrocatalysis provide a nonthermal reaction driving force and reduce the need for hazardous stoichiometric redox reagents and their resultant waste products. A key parameter in electrochemical processes is Faradaic yield, defined as the percentage of electrons used in the desired product.

Electrochemical reduction reactions often require proton equivalents; however, direct reduction of protons to hydrogen lowers the Faradaic yield for the targeted product. The hydrogen evolution reaction (HER) is often thermodynamically favorable (occurs at a lower potential) over many desired reactions. Even in cases where the standard potential for the targeted reaction is positive of the standard hydrogen potential, applied overpotentials often result in exergonic H_2 evolution. The challenge of parasitic H_2 evolution in electrochemical reductions is reflected in the literature; it is cited as the biggest obstacle in electrocatalytic N_2 reduction.[15−19] Additionally, most organic electrosyntheses reported thus far are for oxidation, not reduction, reactions.[1−8]

To achieve greater product selectivity, hydrogen evolution must be suppressed. Electrochemists have long known how to kinetically inhibit H_2 evolution at electrodes using materials with high overpotentials for HER, such as Hg or glassy carbon.[20,21] However, H_2 evolution is kinetically facile with most transition-metal complexes that are used to mediate redox reactivity.

The concomitant evolution of H_2 is particularly acute in CO_2 reduction.[22−26] Direct electrochemical reduction of CO_2 into energy-dense fuels using renewable energy is a convenient method for achieving high-density energy storage. However, the standard potentials for most C-based products are within a few hundred millivolts of the standard hydrogen potential.[27] A few studies on CO_2 reduction have reported inhibition of HER in the presence of local cationic charges. Cationic surfactants and additives are known to suppress HER with heterogeneous catalysts.[28−31] DeLuca et al. also reported improved Faradaic efficiency (FE) for CO_2 reduction to CO when cationic functionalities were appended to a Pd complex, although the isolated impact of the local charge on H^+ reduction was not specifically assessed.[32]

Received: April 2, 2021
Revised: May 21, 2021
Published: June 18, 2021

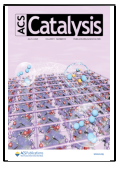

https://doi.org/10.1021/acscatal.1c01527
ACS Catal. 2021, 11, 8155–8164

The use of secondary sphere interactions has been explored in homogeneous electrocatalysts for CO_2 reduction, including a secondary metal,[33] hydrogen-bonding interactions,[34−38] and cationic interactions through ammonium and imidazolium functionalities.[39,40] In these cases, an unmodified catalyst was already selective for CO_2 reduction, and the cooperative interaction accelerated the proposed rate-limiting CO_2 binding and activation steps.

To systematically study the effect of charges on electrocatalytic HER, we synthesized a tridentate ligand with an appended aza-crown cavity (**SNS^{crown}[NaCl]**, Chart 1), which

Chart 1

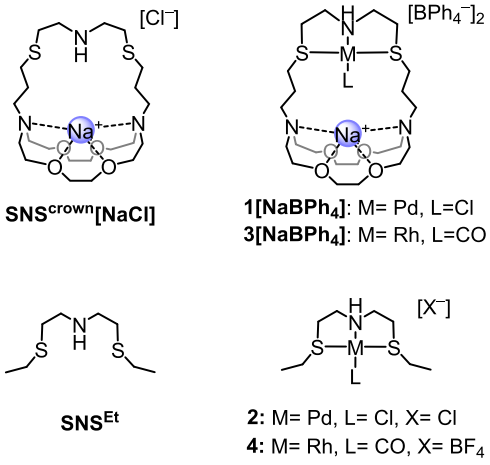

can contain either a Na^+ or Ba^{2+} cation. A ligand without an appended aza-crown cavity was synthesized for comparison (**SNS^{Et}**, Chart 1). We investigated the corresponding Pd complexes for the electrocatalytic HER activity and found increases in overpotential (up to 260 mV) with increasing cationic charge. The increase in overpotential was relatively consistent across multiple acids that span 10 pK_a units and two different solvents (CH_3CN and dimethylformamide, DMF).

Because the presence of a cation suppresses H_2 evolution, we also examined the electrocatalytic activity of the complexes toward CO_2 reduction. Similar Pd complexes with tridentate ligands are known to have electrocatalytic activity toward CO_2 reduction to CO, including the aforementioned study by DeLuca et al.[32,41−48] CO is a valuable target for CO_2 reduction because it can be combined with H_2 to make synthesis gas, which can then be upgraded to liquid fuels. However, the standard potential for direct proton reduction to hydrogen is 68 mV positive (favorable) compared to CO_2 reduction to CO in dimethylformamide ($E°$ = −0.662 and −0.73 V vs $Fe(C_5H_5)_2^{+/0}$, respectively).[26] We found that the presence of Ba^{2+} results in a modest increase in selectivity for CO as a product. Our results were complicated by the decomposition of the Pd complexes under electrolytic conditions. We note that the presence of Ba^{2+} improves stability under reductive conditions. Although our Pd complexes are ultimately unstable under electrolytic CO_2 reduction conditions, our systematic studies on the HER activity with varying cationic charges, acids, and solvents point to a synthetic design strategy to improve product selectivity in reductive catalysis.

RESULTS AND DISCUSSION

Synthesis. The ligand at the focus of our investigation, **SNS^{crown}[NaCl]**, was synthesized in three steps from the previously reported *tert*-butyloxycarbonyl (Boc) protected *N*,*N*′-bis(2-chloroethyl) amine[49] (**A**). Substitution of 3-mercaptopropionic acid with **A** forms the corresponding diacid, **B**. The aza-crown ether chain was then appended to the ligand via amide linkages upon reaction of diaza-18-crown-6 with acid chloride functionalized **B** formed in situ to produce the diamide macrocycle, **C**. Finally, removal of the Boc group and reduction of each amide to their corresponding amine were accomplished in one step by a reaction with borane·tetrahydrofuran followed by acidic workup to form the completed **SNS^{crown}[NaCl]**. The corresponding Pd complex **1[NaBPh$_4$]** was formed by a reaction with $PdCl_2$ followed by salt metathesis with $NaBPh_4$. The Na^+ ions were derived from the workup of the reaction where acidic and basic washes ($NaHSO_4$ and NaOH were used, respectively) of the organic layer were performed during solvent extraction to remove residual starting materials from the crude mixture. The identity and purity of **1[NaBPh$_4$]** were confirmed by ^1H and $^{13}C\{^1H\}$ NMR spectroscopy (Figures S7 and S8), mass spectrometry, and elemental analysis (see Supporting Information, SI). The same procedure was attempted using the corresponding

Scheme 1

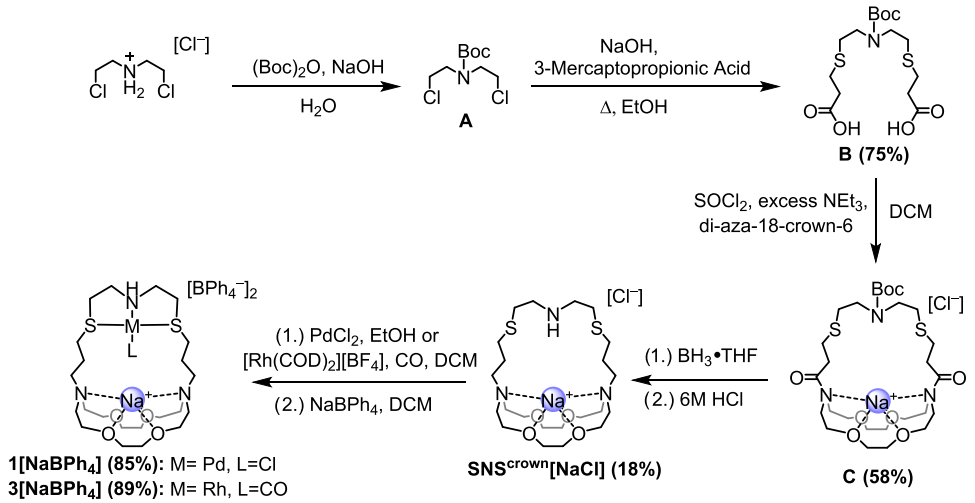

https://doi.org/10.1021/acscatal.1c01527
ACS Catal. 2021, 11, 8155−8164

tetrabutylammonium salts in an attempt to isolate an unmetallated crown ligand; however, the compound could not be cleanly isolated.

The Ba^{2+} derivative ("**1**[Ba^{2+}]") was also prepared because it readily displaces Na^+ in the aza-crown. 1, 10-Diaza-18-crown-6, which is very similar to the aza-crown in $\mathbf{SNS}^{\mathbf{crown}}$, has been shown to have a significant preference for Ba^{2+} over Na^+ ions in DMF[50−56] ($\log(K) = 2.2$ vs 5.55 for Na^+ and Ba^{2+} ions, respectively).[57] The ^{1}H NMR spectra of **1**[$\mathbf{NaBPh_4}$] features significant shifts in the crown ether resonances upon the addition of 1.1 equiv $Ba(OTf)_2$ (Figure S20). The displacement of Na^+ by Ba^{2+} in the aza-crown of **1**[$\mathbf{NaBPh_4}$] is further confirmed by mass spectrometry (Figures S21−S23). Postsynthetic removal of a barium cation from the crown of **1**[Ba^{2+}] was also attempted using guanidine sulfate; however, it was unsuccessful.

To assess the effects of the proximal alkali or alkaline earth metal cations on the reactivity of bound substrates, an analogue without the aza-crown ether functionality was synthesized for comparison. *N*,*N*′-Bis(2-(ethylthio)ethyl)-amine ($\mathbf{SNS}^{\mathbf{Et}}$)[58] and **2**[59] (Chart 1) were prepared. Our revised preparation of **2** (see SI) resulted in a greater yield and a shorter reaction time. The electrochemical properties and small molecule reactivity of **2** had not previously been reported.

Structural Characterization. We were unable to grow crystals of **1**[$\mathbf{NaBPh_4}$] of sufficient quality for structural characterization by X-ray diffraction. Instead, we obtained solid-state structures for the corresponding isoelectronic Rh(I) carbonyl complexes of **1**[$\mathbf{NaBPh_4}$] and **2** to serve as structural models for their Pd(II) counterparts (Scheme 1 and Figure 1). The Rh(I) complexes were synthesized by the addition of a ligand ($\mathbf{SNS}^{\mathbf{crown}}$[**NaCl**] or $\mathbf{SNS}^{\mathbf{Et}}$) to [$Rh(COD)_2$][$BF_4$] in dichloromethane and then sparging the solution with CO gas.

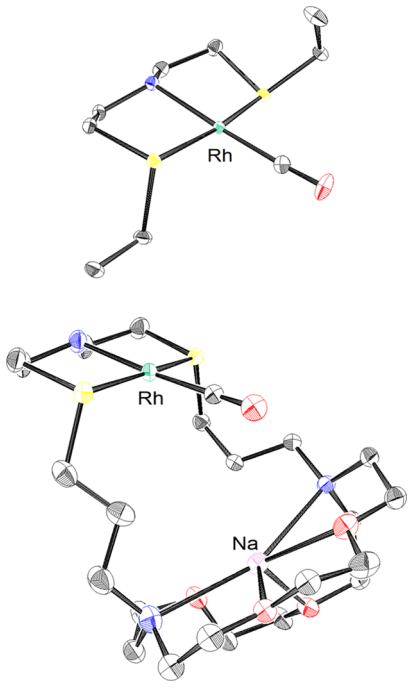

Figure 1. Crystal structures of **4** (top) and **3**[$\mathbf{NaBPh_4}$] (bottom). Hydrogens, counteranions, and solvent molecules are omitted for clarity. Ellipsoids are shown at 50% probability.

The crude products were then extracted with toluene and recrystallized with diethyl ether to obtain the purified products (**3**[**NaCl**] and **4**). The outer-sphere anions of the aza-crown containing the complex (**3**[**NaCl**]) were replaced with tetraphenylborate by salt metathesis of **3**[**NaCl**] with $NaBPh_4$ in DCM to form **3**[$\mathbf{NaBPh_4}$]. The identities of **3**[$\mathbf{NaBPh_4}$] and **4** were confirmed by IR spectroscopy (Figures S13, S16, and S19), ^{1}H and $^{13}C\{^1H\}$ NMR spectroscopy (Figures S11, S12, S14, S15, S17, and S18), mass spectrometry, and elemental analysis.

The solid-state structures of **3**[$\mathbf{NaBPh_4}$] and **4** are shown in Figure 1. Both **3**[$\mathbf{NaBPh_4}$] and **4** feature a square planar Rh metal ion coordinated to an SNS tridentate ligand in a tridentate manner with a CO ligand coordinated trans to the amine nitrogen. **3**[$\mathbf{NaBPh_4}$] features sodium bound to the pendant aza-crown ether moiety with a Rh-Na distance of 5.07 Å. The CO ligand in **3**[$\mathbf{NaBPh_4}$] is disordered over two positions, preventing accurate measurement of the carbon and oxygen distances from the sodium ion. We expect the Rh(I) and Pd(II) centers in the aza-crown complexes **3**[$\mathbf{NaBPh_4}$] and **1**[$\mathbf{NaBPh_4}$] to have similar structures since both are second-row metals with d^8 electron configurations and favor a square planar coordination geometry.

Electronic Absorption and Electrochemical Properties. Electronic absorption data for each Pd complex are listed in Table 1. Both **1** and **2** feature a ligand-to-metal charge-

Table 1. Electronic Absorption Data of Pd Complexes

compound	λ_{max} (ε)[a]
1[$\mathbf{NaBPh_4}$]	316 (sh); 367 (1900)[b]
1[**NaCl**]	~315 (sh); 367 (2340)[c]
1[$\mathbf{NaBPh_4}$] + $Ba(OTf)_2$	316 (sh); 367 (1900)[b]
2	367 (1980)[b]
2 + $Ba(OTf)_2$	367 (2100)[b]

[a]Extinction coefficient recorded in M^{-1} cm^{-1} and wavelength in nanometers (sh = shoulder). [b]Dimethylformamide used as a solvent. [c]Dichloromethane used as a solvent.

transfer (LMCT) band at 367 nm and lack observable d−d transitions in dimethylformamide (DMF) (identical bands are observed in methanol). In the aza-crown ether-containing complexes, switching from chloride to tetraphenylborate counteranions (**1**[**NaCl**] vs **1**[$\mathbf{NaBPh_4}$]) resulted in the growth of a shoulder at 316 nm, while the absorption at 367 nm was unaffected. The absorbance spectra of **1**[$\mathbf{NaBPh_4}$] does not change significantly upon the addition of 1.1 equiv of $Ba(OTf)_2$ (Figures S24−S26).

Cyclic voltammograms (CV) of **2** and **1**[$\mathbf{NaBPh_4}$] in dimethylformamide feature two irreversible reductions between scan rates of 0.05 and 5 V/s under a N_2 atmosphere that we assign as the reduction from Pd(II) to Pd(I) and then to Pd(0). (Figures 2, S27, and S29). The first reductions (E_{PC1}) of **2** and **1**[$\mathbf{NaBPh_4}$] are within 10 mV, while the second reduction (E_{PC2}) for **1**[$\mathbf{NaBPh_4}$] occurs at ~40 mV negative of **2**. Cyclic voltammograms of **1**[$\mathbf{NaBPh_4}$] with 1.1 equiv of barium triflate ($Ba(OTf)_2$) did not show significant changes to either reduction event (Figure 2). These values are also tabulated in Table 2. The oxidation event at −0.4 V for **2** is attributed to a Pd dimer that forms upon reduction (see Dimerization upon Reduction section). Although all of the Pd complexes dimerize upon reduction, the reaction is fastest for **2** and is thus the only one observed in Figure 2.

https://doi.org/10.1021/acscatal.1c01527
ACS Catal. 2021, 11, 8155−8164

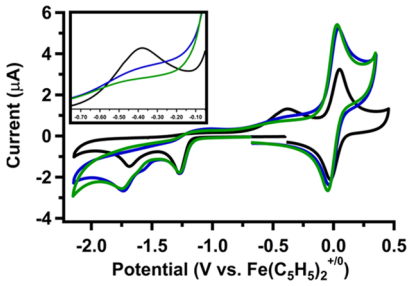

Figure 2. Cyclic voltammograms of 1 mM solutions of **2** (−), **1**[**NaBPh$_4$**] (blue line), and **1**[**NaBPh$_4$**] with 1.1 equiv added Ba(OTf)$_2$ (green line) under a N_2 atmosphere in DMF. The inset features a zoomed-in region of the broad oxidation centered at approximately −0.4 V. The reversible couple centered at 0.0 V corresponds to $Fe(C_5H_5)_2^{+/0}$ internal standard. Scans were recorded at 100 mV/s.

The similarity of the LMCT band energies and molar absorptivities for **2** and **1**[**NaBPh$_4$**], along with their nearly identical Pd(II/I) reduction potentials (E_{PC1}), suggests that the electronic structure of the Pd is not significantly perturbed by the presence of a proximal mono- or dication.

These findings contrast with our investigations with related complexes featuring a crown ether-appended salen ligand.[60−63] In the salen complexes, the presence and charge of the cations significantly modify the redox potential. For those complexes, the metals are within 4.0 Å of each other and share two μ-oxo ligands. For the ligand system described in this work, the metals are likely too far apart (>5.0 Å) to significantly modify the properties of the Pd center. Miller[64] and Gilbertson[65] have reported heterobimetallic metal complexes with flexible appended crowns similar to the compounds discussed herein. They also noted that occupation of the aza-crown with alkali or alkaline earth metals did not significantly affect the spectroscopic or electrochemical properties of the redox-active metal.

Reactivity with H$^+$. To investigate the impact of the proximal cations on proton reduction, solutions of **1**[**NaBPh$_4$**] and **2** were titrated with the following Brønsted acids in dimethylformamide and CH$_3$CN: [Et$_3$NH][BF$_4$] (pK_a(CH$_3$CN) = 18.8), protonated 1,8-diazabicyloundec-7-ene, [HDBU][BF$_4$] (pK_a(CH$_3$CN) = 24.3), protonated 1,5,7-trazabicyclodec-5-ene, [HTBD][BF$_4$] (pK_a(CH$_3$CN) = 26.0), and phenol (pK_a(CH$_3$CN) = 29.1).[9,66] The acids were selected because they span 10 pK_a units and include both cationic and neutral acids. To ensure that the complexes are stable in the presence of acid, UV−vis titrations of **2** with the strongest acid [HNEt$_3$][BF$_4$] in DMF was performed. No changes were observed after up to 20 equiv of acid were added (both with and without added Ba(OTf)$_2$, Figure S39) and, indicating no protonation occurs in the Pd(II) complexes prior to reduction.

For all of these acids, a new reductive peak appears negative of the first reduction (E_{PC1}). This new event ($E_{PC}^{H^+}$) is attributed to proton reduction by the Pd complex, as it is not present in the absence of an acid, nor in the absence of **1**[**NaBPh$_4$**] or **2**. Additionally, the current of $E_{PC}^{H^+}$ increases with increasing concentration of acid, consistent with electrocatalysis (Figure S31).

The onset potential for H$^+$ reduction ($E_{PC}^{H^+}$) in DMF with each acid for **1**[**NaBPh$_4$**] is shifted negative (up to 170 mV) compared to **2** (Table 3, Figures 3 and S33−S37). This anodic shift corresponds to a higher catalytic overpotential. Addition of 1.1 equiv of Ba(OTf)$_2$ to **1**[**NaBPh$_4$**] results in an even larger shift (up to 260 mV) in $E_{PC}^{H^+}$. This trend is consistent across a range of acid concentrations with each of the acids examined except [HDBU][BF$_4$] in CH$_3$CN (Table 3 and Figures S33−S37). The magnitude of the cathodic shift correlates with the charge of the bound cation, as larger shifts in $E_{PC}^{H^+}$ were generally observed switching from monovalent to divalent cations. In DMF, the addition of neutral phenol maintained the cathodic shift in onset potential. There are some changes in the cyclic voltammograms between solvents. These changes may be due to the large difference in standard potential for hydrogen evolution between the two solvents (−0.028 vs −0.662 V vs Fc for MeCN and DMF, respectively)[26] or their different solvent donor numbers.[67]

No shift in $E_{PC}^{H^+}$ occurs upon addition of 2.2 equiv of Ba(OTf)$_2$ to a solution of **2** (solid black vs dotted green trace, Figure 3). This result the cathodic shifts with **SNS^{crown}** complexes are not a result of free alkali or alkaline earth metal cations in solution, but rather bound cations in the aza-crown cavity. Proton reduction to produce H_2 was confirmed using controlled potential electrolysis. A 1 mM solution of **2** in DMF containing 10 mM triethylammonium tetrafluoroborate ([HNEt$_3$][BF$_4$]) was held at −1.40 V vs $Fe(C_5H_5)_2^{+/0}$ for about 15 min. A total of −1.69 C of charge was passed, corresponding to 2.9 turnovers (Figure S32). Gas chromatography (GC) confirmed the production of H_2 in the headspace with 77 ± 4% Faradaic efficiency (FE) with no other identifiable products. The balance of charge not contributing to H$^+$ reduction likely accounts for catalyst decomposition. During the course of the electrolysis, there was a drop in catalytic current that coincided with a color change of the solution and formation of black precipitate.

Most molecular electrocatalysts generate hydrogen through formation of a hydride intermediate which is then protonated.[68] We hypothesize that proton reduction is inhibited due to electrostatic repulsion between the acid and the positively charged aza-crown ether portion of the complex. The electrostatic repulsion may disfavor formation of a metal

Table 2. Electrochemical Data of Pd Complexes

compound	$^a E_{PCl}^{N2}$ (E_{PCl}^{CO2})	$^a E_{PC2}^{N2}$ (E_{PC2}^{CO2})	$^a E_{PC3}^{N2}$ (E_{PC3}^{CO2})
1[**NaBPh$_4$**]	−1.27 (−1.27)	−1.74 (−1.74)	≈−2.50^b (−1.89)
1[**NaCl**]	−1.27	−1.73	
1[**NaBPh$_4$**] + Ba(OTf)$_2$	−1.27 (−1.27)	−1.74 (−1.80)	−2.58^b
2	−1.28 (−1.28)	−1.70 (−1.63)	−2.30^b (−1.92)
2 + Ba(OTf)$_2$	−1.28 (−1.28)	−1.64 (−1.58)	−1.75

^{a}Potential measured as *V* vs $Fe(C_5H_5)_2^{+/0}$ in dimethylformamide using 0.200 M TBAPF6 as a supporting electrolyte. The scan rate was 100 mV/s for each measurement using a glassy carbon working electrode. ^{b}Recorded at a 25 mV/s scan rate.

https://doi.org/10.1021/acscatal.1c01527
ACS Catal. 2021, 11, 8155−8164

Table 3. Cation Effects on Proton Reduction by 1 with Various Acids in Dimethylformamide and Acetonitrile

			dimethylformamide (DMF)		acetonitrile (CH_3CN)	
acid	pK_a[a]	cation	[HA] (mM)	shift from **2** ($\Delta E_{PC}^{H^+}$, mV)	[HA] (mM)	shift from **2** ($\Delta E_{PC}^{H^+}$, mV)
$[HNEt_3][BF_4]$	18.8	Na^+	2	170	10	150
		Ba^{2+}	2	220	10	260
$[HDBU][BF_4]$	24.3	Na^+	40	60	10	0
		Ba^{2+}	40	140	10	190
$[HTBD][BF_4]$	26.0	Na^+	20	60	20	170
		Ba^{2+}	20	100	20	210
phenol	29.0	Na^+	40	160		
		Ba^{2+}	40	260		

[a] pK_a values are reported in MeCN.[9,25]

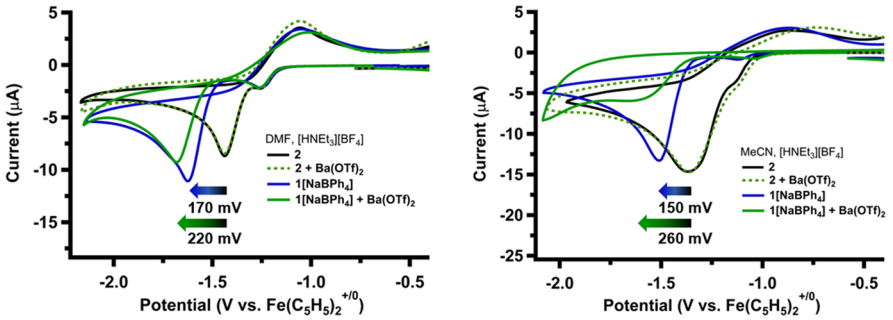

Figure 3. Cyclic voltammograms of 1.00 mM solutions of **1**[**NaBPh$_4$**] and **2** with 2 equiv $[HNEt_3][BF_4]$ in DMF (left), and 10 equiv $[HNEt_3][BF_4]$ in MeCN (right). **1**[**NaBPh$_4$**] solutions are shown without added alkali or alkaline earth metal (blue line) and with 1.1 equiv added $Ba(OTf)_2$ (green line). Solutions of **2** are shown with (green dotted line) and without (−) 2.2 equiv added $Ba(OTf)_2$. Scans were recorded at 100 mV/s.

hydride intermediate and/or protonation of the hydride to form an H−H bond. As a result, more reducing species must be accessed for proton reduction to occur, which changes the mechanisms for catalysis, effectively increasing the overpotential.

Reactivity with CO_2. Because the presence of an alkali or alkaline earth metal in the aza-crown cavity increases the overpotential for H^+ reduction, we next investigated whether we could capitalize on this effect to improve the selectivity (Faradaic efficiency) for CO_2 reduction reactions. When solutions of **1**[**NaBPh$_4$**] and **2** are reduced under 1 atm of CO_2 in DMF, they display a new irreversible reduction (E_{PC3}^{CO2} = −1.89 and −1.92 V vs $(C_5H_5)_2Fe^{+/0}$, respectively, Figure 4, values tabulated in Table 2). The first two reduction events remain diffusion limited and are irreversible up to scan rates of 1000 mV/s (Figures S40−S43). Additionally, each complex displays enhanced current at the second reduction, which suggests CO_2 binding occurs upon reduction. The oxidation event (E_{PA}) under N_2 for each complex disappears under a CO_2 atmosphere, although **2** displays a new oxidation event at 0.28 V vs $Fe(C_5H_5)_2^{+/0}$ under CO_2. The differences in the cyclic voltammograms suggest CO_2 binding upon reduction to Pd(0) (and consequent rereduction), or an EECE process, with **1**[**NaBPh$_4$**] and **2**. This conclusion is further supported by variable scan rate studies. The peak current of the third reduction for **1**[**NaBPh$_4$**] and **2** under CO_2, normalized by dividing by the square root of the scan rate ($[i_{PC3}]/[\nu^{1/2}]$), decreases with the increasing scan rate (Figure S44), indicating EECE-type behavior.[69] The reaction with CO_2 appears slower with **1**[**NaBPh$_4$**] than with **2**, as the third reduction event (E_{PC3}^{CO2}) is no longer present at scan rates above 1 V/s with **1**[**NaBPh$_4$**], whereas it is still prominent at the same scan rate with solutions of **2**. Similar

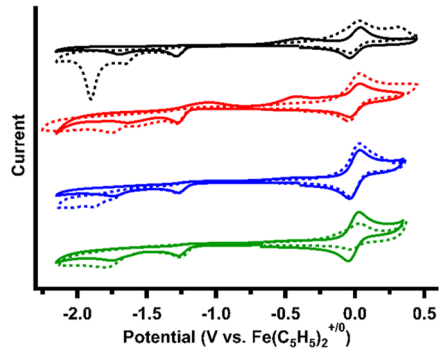

Figure 4. Cyclic voltammograms of 1.00 mM solutions of **2** (−), **2** + 1.1 equiv $Ba(OTf)_2$ (red line), **1**[**NaBPh$_4$**] (blue line), and **1**[**NaBPh$_4$**] + 1.1 equiv $Ba(OTf)_2$ (green line) in dimethylformamide under a N_2 (solid) or CO_2 (dashed) atmosphere. Scans were recorded at 100 mV/s. The reversible peak centered at 0.0 V corresponds to $Fe(C_5H_5)_2^{+/0}$ internal standard.

behavior occurs when 1.1 equiv of barium triflate is added to a solution of **1**[**NaBPh$_4$**] to form the putative Ba^{2+} complex under a CO_2 atmosphere. (Figure 4).

The lower reactivity of **1**[**NaBPh$_4$**] toward CO_2 compared to **2** may be due, in part, to increased steric hindrance, which is known to diminish the reactivity in other complexes with tridentate complexes.[70,71] The further decrease in the CO_2 reactivity when $Ba(OTf)_2$ is added to **1**[**NaBPh$_4$**] suggests that steric hindrance may not be the only reason, as the steric bulk of the barium and sodium bound species should be similar (the ionic radii for Na^+ and Ba^{2+} are 1.86 and 2.22 Å, respectively).

Although the **SNS^{crown}** complexes do not show large shifts in the onset potential for CO_2 reduction compared to **2**, the cationic shift in the onset of H^+ reduction afforded by the

https://doi.org/10.1021/acscatal.1c01527
ACS Catal. 2021, 11, 8155−8164

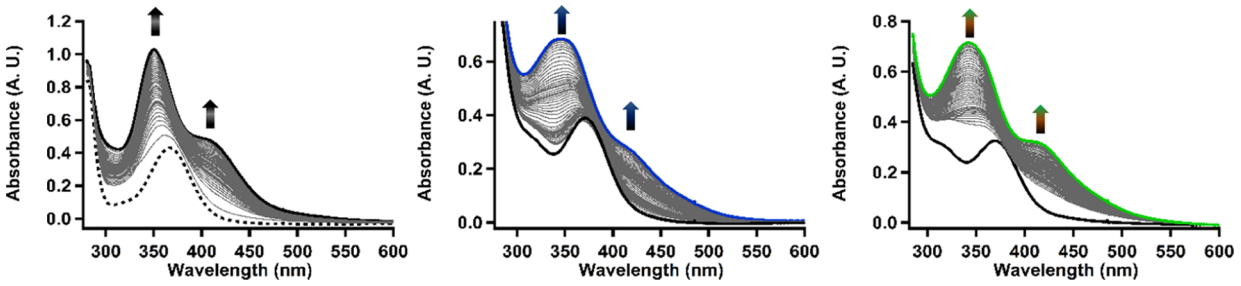

Figure 5. Electronic absorption spectra for dimerization reactions of **2** (left), **1**[**NaBPh$_4$**] (middle), and **1**[**NaBPh$_4$**] + Ba(OTf)$_2$ (right) over time to form the corresponding dimeric Pd^{I} species (where black trace is t = 0 and endpoints are −, blue line, and green line respectively).

SNS^{crown} complexes could promote product selectivity vs **2** under proper conditions. To test this hypothesis, titrations with various acid sources were performed under N_2 and CO_2 atmospheres in DMF. From these investigations, [HDBU][BF_4] was selected as the acid of choice because it showed the largest increase in the reductive current under CO_2 compared to N_2 (Figures S46−S49).

Controlled potential electrolysis of a 1 mM solution of **2** under a CO_2 atmosphere containing 40 mM [HDBU][BF_4] in DMF at −1.75 V vs $Fe(C_5H_5)_2^{+/0}$ produced H_2 as the sole product after 5.2 turnovers (−5.51 Coulombs passed, Figure S50); the Faradaic efficiency for H_2 was determined to be 43 ± 4%. No CO was detected in the headspace via GC, and ^{1}H NMR of the postelectrolysis solution confirmed that no formate was produced. Similar to the H^+ reduction studies previously described, the low Faradaic efficiency for HER was a result of catalyst decomposition, exhibited by a color change and formation of a black precipitate over time. Decomposition was confirmed by significant changes to cyclic voltammograms and electronic absorption spectra of the pre- vs postelectrolysis solutions (Figure S51).

Similar to electrolysis with **2**, controlled potential electrolysis of a 1 mM solution of **2** + 1.1 equiv Ba(OTf)$_2$ containing 40 mM [HDBU][BF_4] in DMF under a CO_2 atmosphere at −1.75 V vs $Fe(C_5H_5)_2^{+/0}$ produced H_2 as the sole product after 6.1 turnovers (−8.66 Coulombs passed, Figure S52); the Faradaic efficiency for H_2 was determined to be 90 ± 10%. No CO was detected in the headspace via GC, and ^{1}H NMR of the postelectrolysis solution confirmed that no formate was produced. Although only minor precipitate formation was observed, **2** was no longer observable in the postelectrolysis solution via cyclic voltammetry or electronic absorption spectroscopy, indicating catalyst decomposition (Figure S53). Electrolysis of a 1 mM solution of **1**[**NaBPh$_4$**] + 1.1 equiv Ba(OTf)$_2$ under the same conditions resulted in the production of both H_2 and CO with Faradaic efficiencies of 88 ± 8 and 6 ± 1%, respectively, after 2.7 turnovers (−2.57 Coulombs passed); no production of formate was detected via ^{1}H NMR (Figure S54). Although the current decreases over the course of electrolysis, cyclic voltammograms and electronic absorption spectra of the pre- and postelectrolysis solutions indicate that significantly less decomposition occurred compared to **2** under the same catalytic conditions (Figure S55 vs S51, S53, and S56). The difference in CO production with **1**[**NaBPh$_4$**] + 1 equiv Ba(OTf)$_2$ compared to **2** supports the hypothesis that a proximal cation acts to hinder proton reduction in favor of CO_2 reduction. Each electrolysis was performed over a pool of mercury to preclude the formation of Pd nanoparticles. However, partial catalyst decomposition occurred in both experiments, preventing unequivocal assignment of the catalytically active species.

An unexpected result of the electrolysis was the increased stability of **1**[**NaBPh$_4$**] vs **2** during catalysis. Although less current was passed in the electrolysis of the **SNS^{crown}** complex compared to **2**, similar quantities of product were produced while incurring far less decomposition in the process.

Dimerization upon Reduction. One likely decomposition pathway is dimer formation to produce insoluble or catalytically inactive species. DuBois and co-workers previously found that similar Pd complexes featuring PNP or triphosphine ligands often dimerize upon reduction of the metal center.[33,42,70,72−75] Dimer formation significantly hindered CO_2 reduction with these complexes and served as the primary decomposition pathway under catalytic conditions. At slow scan rates, the complexes displayed a new reduction peak at potentials negative of the Pd$^{I/0}$ reduction under a N_2 atmosphere. These new features were attributed to the reduction of Pd^{I}−Pd^{I} dimers formed in solution.

A similar reduction event (E_{PC3}^{N2}, Table 2) is observed with **2** and the **SNS^{Crown}** complexes under N_2 when scanning negative of the Pd(I/0) reduction event (E_{PC2}) at slow scan rates ($\nu \leq 250$ mV/s, Figure S57). The relative intensity of this third reduction ($[i_{PC3}^{N2}]/[\nu^{1/2}]$) decreases as the scan rate is increased, indicating that it corresponds to the reduction of a product formed in the solution as a result of a previous reduction. The observation of a third reduction event featuring this behavior is consistent with those reported by DuBois et al.

An oxidation event after reduction under N_2 also provides evidence for dimer formation. After the first or second reduction events, a broad oxidation feature appears ($E_{PA} \approx$ −0.4 V vs $Fe(C_5H_5)_2^{+/0}$, Figures 2 and S58−S60). Variable scan rate studies indicate that the peak current over the square root of the scan rate ($[i_{PA}]/[\nu^{1/2}]$) steadily decreases as scan rate is increased (Figure S61). The scan-rate-dependent data for both new features (E_{PC3}^{N2} and E_{PA}) indicate they are associated with the product formed upon reduction (EC) and are consistent with prior reports of dimerization.[69,76]

With **2**, there is evidence of dimerization after both the first and second reductions (Figure S59). In contrast, **1**[**NaBPh$_4$**] with and without added Ba(OTf)$_2$ does not feature this oxidation after being singly reduced, even at scan rates as low as 10 mV/s (Figure S60). Data suggest that the putative dimer does not form quickly upon reduction to Pd(I). When scanning past the second reduction (E_{PC2}), the oxidation event assigned to the dimer increases in intensity in the order: **2** > **1**[**NaBPh$_4$**] > **1**[**NaBPh$_4$**] + Ba(OTf)$_2$. Dimer formation of Pd(I) species upon reduction of the parent Pd(II) complexes was initially investigated using spectroelectrochemical UV−vis spectroscopy (SEC UV−vis). Reduction of **1**[**NaBPh$_4$**] and

https://doi.org/10.1021/acscatal.1c01527
ACS Catal. 2021, 11, 8155−8164

1[**NaBPh$_4$**] + Ba(OTf)$_2$ resulted in the formation of species featuring strong absorbance bands at 345 and 420 nm when a −1.27 V (vs $Fe(C_5H_5)_2^{+/0}$) potential was applied (Figures S62 and S63). A strong absorption band at around 400 nm is characteristic of Pd dimers and has been attributed to arise from the Pd−Pd bond.[42,72,77,78] Both SEC UV−vis experiments feature isosbestic points, indicating the dimer is produced cleanly upon one electron reduction. However, when SEC UV−vis of **2** was performed, the complex decomposed before dimer formation, resulting in formation of a black precipitate.

Dimer formation was also observed by UV−visible spectroscopy using stoichiometric reductants. Reduction of **2** with 1 equiv of $Co(C_5H_5)_2$ in DMF ($E_{1/2}$ = −1.33 V vs $Fe(C_5H_5)_2^{+/0}$ in DMF, Figure S64) at room temperature resulted in the formation of a bright yellow solution. The new species features charge-transfer bands at 350 and 420 nm with molar absorptivities of 18 460 and 8760 M^{-1} cm^{-1}, respectively (Figure S65). The position and intensity of the absorptions are consistent with dimer formation and closely match the SEC UV−vis spectra obtained for **1**[**NaBPh$_4$**] and **1**[**NaBPh$_4$**] + Ba(OTf)$_2$.

The relative rates of dimerization for each complex were determined via UV−visible spectroscopy using 1 equiv of $Co(C_5H_5)_2$ in DMF at −40 °C (Figure 5). The second-order rate constants (k_{obs}) were determined to be 139 ± 3, 61 ± 2, and 44 ± 2 M^{-1} s^{-1} for **2**, **1**[**NaBPh$_4$**], and **1**[**NaBPh$_4$**] + Ba(OTf)$_2$, respectively (Figures S67−S69). The measured rate constants are consistent with the overall intensities of E_{PA} for each complex discussed previously (Figure 2, inset). Part of the decrease in the rate between **2** and **1**[**NaBPh$_4$**] may be due to the increased steric hindrance of **1**[**NaBPh$_4$**]. However, the decrease in rate when a higher charge (Ba^{2+}) cation is added to **1**[**NaBPh$_4$**] implies that sterics are not the only cause. Electrostatic repulsion is also likely playing a role since the steric bulk of **1**[**NaBPh$_4$**] should remain the same between the two cation-bound species.

The formation of metal−metal dimers is a common decomposition pathway for CO_2 reduction catalysts.[33,43,79,80] Incorporation of sterically bulky groups has been shown to inhibit off-cycle dimerization.[42,70,79,81−83] However, these modifications can result in undesirable changes to the electronic structure or activity of the catalyst.[70,71] Our results indicate that the addition of charge provides another strategy to avoid dimerization reactions, which has previously been shown to inhibit the rate of bimolecular manganese nitride coupling reactions.[60]

CONCLUSIONS

A series of Pd and Rh SNS complexes with and without pendant aza-crown ether moieties bound to S-block metal cations were synthesized and characterized. The Rh(I) systems were crystallographically characterized to gain structural insight into their isoelectronic Pd(II) counterparts. For the Pd(II) complexes with Na^+ or Ba^{2+} in the aza-crown, there was a cathodic shift in the potential for the electrocatalytic hydrogen evolution reaction (HER), corresponding to an increase in overpotential. The shift was larger for Ba^{2+} than Na^+ and was evident with a range of cationic and neutral acid sources that span 10 pK_a units in both CH_3CN and dimethylformamide.

When Ba^{2+} was present in the aza-crown, the Pd complexes exhibited greater activity toward the electrolytic reduction of CO_2 and improved product selectivity for CO (Faradaic yield). Unfortunately, instability of the reduced forms of each complex resulted in decomposition under prolonged electrolysis. We found evidence that dimerization plays a predominant role in decomposition, which has been reported in similar Pd complexes. Although increasing the cationic charge slows this deactivation pathway, it still occurs at a sufficient rate to impede catalysis.

Although the Pd complexes described herein were unstable to reduction, our results indicate a strategy to improve selectivity for electrochemical reduction reactions by inhibiting proton reduction. A key element of this strategy is the distance at which a proximal S-block metal is incorporated into a ligand framework. It is sufficiently far from the transition metal to have negligible effects on the electronic structure of the Pd center, while having profound impacts on its reactivity. We postulate that the cationic charge inhibits HER through electrostatic interactions with charged protons and thus should not generally inhibit the approach of neutral substrates, such as CO_2.

ASSOCIATED CONTENT

Supporting Information

The Supporting Information is available free of charge at https://pubs.acs.org/doi/10.1021/acscatal.1c01527.

Experimental details, spectroscopic data, and electrochemical data (PDF)

Crystallographic data (CIF)

Crystallographic data (CIF)

AUTHOR INFORMATION

Corresponding Author

Jenny Y. Yang − *Department of Chemistry, University of California, Irvine, California 92697, United States;* orcid.org/0000-0002-9680-8260; Email: j.yang@uci.edu

Authors

Jeffrey M. Barlow − *Department of Chemistry, University of California, Irvine, California 92697, United States*

Joseph W. Ziller − *Department of Chemistry, University of California, Irvine, California 92697, United States;* orcid.org/0000-0001-7404-950X

Complete contact information is available at: https://pubs.acs.org/10.1021/acscatal.1c01527

Notes

The authors declare no competing financial interest.

ACKNOWLEDGMENTS

The authors would like to acknowledge support from the NSF Award (CHE-1554744 and CHE-2102589). J.Y.Y. is grateful for support as a Sloan Foundation Fellow, a Camille Dreyfus Teacher-Scholar, and a CIFAR Azrieli Global Scholar in the Bio-Inspired Energy Program.

REFERENCES

(1) Pollok, D.; Waldvogel, S. R. Electro-organic synthesis—a 21st century technique. *Chem. Sci.* **2020**, *11*, No. 12386.

(2) Horn, E. J.; Rosen, B. R.; Baran, P. S. Synthetic Organic Electrochemistry: An Enabling and Innately Sustainable Method. *ACS Cent. Sci.* **2016**, *2*, 302−308.

(3) Kärkäs, M. D. Electrochemical strategies for C−H functionalization and C−N bond formation. *Chem. Soc. Rev.* **2018**, *47*, 5786−5865.

(4) Waldvogel, S. R.; Janza, B. Renaissance of Electrosynthetic Methods for the Construction of Complex Molecules. *Angew. Chem., Int. Ed.* **2014**, *53*, 7122−7123.
(5) Wiebe, A.; Gieshoff, T.; Möhle, S.; Rodrigo, E.; Zirbes, M.; Waldvogel, S. R. Electrifying Organic Synthesis. *Angew. Chem., Int. Ed.* **2018**, *57*, 5594−5619.
(6) Yoshida, J.-i.; Kataoka, K.; Horcajada, R.; Nagaki, A. Modern Strategies in Electroorganic Synthesis. *Chem. Rev.* **2008**, *108*, 2265−2299.
(7) Yan, M.; Kawamata, Y.; Baran, P. S. Synthetic Organic Electrochemical Methods Since 2000: On the Verge of a Renaissance. *Chem. Rev.* **2017**, *117*, 13230−13319.
(8) Waldvogel, S. R.; Lips, S.; Selt, M.; Riehl, B.; Kampf, C. J. Electrochemical Arylation Reaction. *Chem. Rev.* **2018**, *118*, 6706−6765.
(9) Kaljurand, I.; Kütt, A.; Sooväli, L.; Rodima, T.; Mäemets, V.; Leito, I.; Koppel, I. A. Extension of the Self-Consistent Spectrophotometric Basicity Scale in Acetonitrile to a Full Span of 28 pKa Units: Unification of Different Basicity Scales. *J. Org. Chem.* **2005**, *70*, 1019−1028.
(10) Lewis, N. S.; Nocera, D. G. Powering the planet: Chemical challenges in solar energy utilization. *Proc. Natl. Acad. Sci. U.S.A.* **2006**, *103*, 15729−15735.
(11) Harriman, A. Prospects for conversion of solar energy into chemical fuels: the concept of a solar fuels industry. *Philos. Trans. R. Soc., A* **2013**, *371*, No. 20110415.
(12) Ganesh, I. Solar fuels vis-à-vis electricity generation from sunlight: The current state-of-the-art (a review). *Renewable Sustainable Energy Rev.* **2015**, *44*, 904−932.
(13) Proppe, A. H.; Li, Y. C.; Aspuru-Guzik, A.; Berlinguette, C. P.; Chang, C. J.; Cogdell, R.; Doyle, A. G.; Flick, J.; Gabor, N. M.; van Grondelle, R.; Hammes-Schiffer, S.; Jaffer, S. A.; Kelley, S. O.; Leclerc, M.; Leo, K.; Mallouk, T. E.; Narang, P.; Schlau-Cohen, G. S.; Scholes, G. D.; Vojvodic, A.; Yam, V. W.-W.; Yang, J. Y.; Sargent, E. H. Bioinspiration in light harvesting and catalysis. *Nat. Rev. Mater.* **2020**, *5*, No. 828.
(14) He, J.; Janáky, C. Recent Advances in Solar-Driven Carbon Dioxide Conversion: Expectations versus Reality. *ACS Energy Lett.* **2020**, *5*, 1996−2014.
(15) Guo, X.; Gu, J.; Lin, S.; Zhang, S.; Chen, Z.; Huang, S. Tackling the Activity and Selectivity Challenges of Electrocatalysts toward the Nitrogen Reduction Reaction via Atomically Dispersed Biatom Catalysts. *J. Am. Chem. Soc.* **2020**, *142*, 5709−5721.
(16) Fan, L.; Xia, C.; Yang, F.; Wang, J.; Wang, H.; Lu, Y. Strategies in catalysts and electrolyzer design for electrochemical CO_2 reduction toward C_{2+} products. *Sci. Adv.* **2020**, *6*, No. eaay3111.
(17) Chen, G.-F.; Ren, S.; Zhang, L.; Cheng, H.; Luo, Y.; Zhu, K.; Ding, L.-X.; Wang, H. Advances in Electrocatalytic N2 Reduction—Strategies to Tackle the Selectivity Challenge. *Small Methods* **2019**, *3*, No. 1800337.
(18) Wang, H.; Chen, Y.; Fan, R.; Chen, J.; Wang, Z.; Mao, S.; Wang, Y. Selective Electrochemical Reduction of Nitrogen to Ammonia by Adjusting the Three-Phase Interface. *Research* **2019**, *2019*, No. 1401209.
(19) Fenwick, A. Q.; Gregoire, J. M.; Luca, O. R. Electrocatalytic Reduction of Nitrogen and Carbon Dioxide to Chemical Fuels: Challenges and Opportunities for a Solar Fuel Device. *J. Photochem. Photobiol., B* **2015**, *152*, 47−57.
(20) Felton, G. A. N.; Glass, R. S.; Lichtenberger, D. L.; Evans, D. H. Iron-Only Hydrogenase Mimics. Thermodynamic Aspects of the Use of Electrochemistry to Evaluate Catalytic Efficiency for Hydrogen Generation. *Inorg. Chem.* **2006**, *45*, 9181−9184.
(21) Chen, J. G.; Crooks, R. M.; Seefeldt, L. C.; Bren, K. L.; Bullock, R. M.; Darensbourg, M. Y.; Holland, P. L.; Hoffman, B.; Janik, M. J.; Jones, A. K.; Kanatzidis, M. G.; King, P.; Lancaster, K. M.; Lymar, S. V.; Pfromm, P.; Schneider, W. F.; Schrock, R. R. Beyond fossil fuel−driven nitrogen transformations. *Science* **2018**, *360*, No. eaar6611.
(22) Garg, S.; Li, M.; Weber, A. Z.; Ge, L.; Li, L.; Rudolph, V.; Wang, G.; Rufford, T. E. Advances and challenges in electrochemical CO2 reduction processes: an engineering and design perspective looking beyond new catalyst materials. *J. Mater. Chem. A* **2020**, *8*, 1511−1544.
(23) Birdja, Y. Y.; Pérez-Gallent, E.; Figueiredo, M. C.; Göttle, A. J.; Calle-Vallejo, F.; Koper, M. T. M. Advances and challenges in understanding the electrocatalytic conversion of carbon dioxide to fuels. *Nat. Energy* **2019**, *4*, 732−745.
(24) Sun, Z.; Ma, T.; Tao, H.; Fan, Q.; Han, B. Fundamentals and Challenges of Electrochemical CO2 Reduction Using Two-Dimensional Materials. *Chem* **2017**, *3*, 560−587.
(25) Resasco, J.; Bell, A. T. Electrocatalytic CO2 Reduction to Fuels: Progress and Opportunities. *Trends Chem.* **2020**, *2*, 825−836.
(26) Pegis, M. L.; Roberts, J. A. S.; Wasylenko, D. J.; Mader, E. A.; Appel, A. M.; Mayer, J. M. Standard Reduction Potentials for Oxygen and Carbon Dioxide Couples in Acetonitrile and N,N-Dimethylformamide. *Inorg. Chem.* **2015**, *54*, 11883−11888.
(27) Zhang, W.; Hu, Y.; Ma, L.; Zhu, G.; Wang, Y.; Xue, X.; Chen, R.; Yang, S.; Jin, Z. Progress and Perspective of Electrocatalytic CO2 Reduction for Renewable Carbonaceous Fuels and Chemicals. *Adv. Sci.* **2018**, *5*, No. 1700275.
(28) Sarkar, S.; Maitra, A.; Banerjee, S.; Thoi, V. S.; Dawlaty, J. M. Electric Fields at Metal−Surfactant Interfaces: A Combined Vibrational Spectroscopy and Capacitance Study. *J. Phys. Chem. B* **2020**, *124*, 1311−1321.
(29) Banerjee, S.; Han, X.; Thoi, V. S. Modulating the Electrode−Electrolyte Interface with Cationic Surfactants in Carbon Dioxide Reduction. *ACS Catal.* **2019**, *9*, 5631−5637.
(30) Quan, F.; Xiong, M.; Jia, F.; Zhang, L. Efficient electroreduction of CO2 on bulk silver electrode in aqueous solution via the inhibition of hydrogen evolution. *Appl. Surf. Sci.* **2017**, *399*, 48−54.
(31) Thorson, M. R.; Siil, K. I.; Kenis, P. J. A. Effect of Cations on the Electrochemical Conversion of CO2 to CO. *J. Electrochem. Soc.* **2013**, *160*, F69−F74.
(32) DeLuca, E. E.; Xu, Z.; Lam, J.; Wolf, M. O. Improved Electrocatalytic CO2 Reduction with Palladium bis(NHC) Pincer Complexes Bearing Cationic Side Chains. *Organometallics* **2019**, *38*, 1330−1343.
(33) Steffey, B. D.; Curtis, C. J.; DuBois, D. L. Electrochemical Reduction of CO2 Catalyzed by a Dinuclear Palladium Complex Containing a Bridging Hexaphosphine Ligand: Evidence for Cooperativity. *Organometallics* **1995**, *14*, 4937−4943.
(34) Chapovetsky, A.; Do, T. H.; Haiges, R.; Takase, M. K.; Marinescu, S. C. Proton-Assisted Reduction of CO2 by Cobalt Aminopyridine Macrocycles. *J. Am. Chem. Soc.* **2016**, *138*, 5765−5768.
(35) Chapovetsky, A.; Welborn, M.; Luna, J. M.; Haiges, R.; Miller, T. F.; Marinescu, S. C. Pendant Hydrogen-Bond Donors in Cobalt Catalysts Independently Enhance CO2 Reduction. *ACS Cent. Sci.* **2018**, *4*, 397−404.
(36) Froehlich, J. D.; Kubiak, C. P. Homogeneous CO2 Reduction by Ni(cyclam) at a Glassy Carbon Electrode. *Inorg. Chem.* **2012**, *51*, 3932−3934.
(37) DuBois, D. L. Development of Molecular Electrocatalysts for Energy Storage. *Inorg. Chem.* **2014**, *53*, 3935−3960.
(38) Beley, M.; Collin, J. P.; Ruppert, R.; Sauvage, J. P. Electrocatalytic reduction of carbon dioxide by nickel cyclam2+ in water: study of the factors affecting the efficiency and the selectivity of the process. *J. Am. Chem. Soc.* **1986**, *108*, 7461−7467.
(39) Azcarate, I.; Costentin, C.; Robert, M.; Savéant, J.-M. Through-Space Charge Interaction Substituent Effects in Molecular Catalysis Leading to the Design of the Most Efficient Catalyst of CO2-to-CO Electrochemical Conversion. *J. Am. Chem. Soc.* **2016**, *138*, 16639−16644.
(40) Sung, S.; Kumar, D.; Gil-Sepulcre, M.; Nippe, M. Electrocatalytic CO2 Reduction by Imidazolium-Functionalized Molecular Catalysts. *J. Am. Chem. Soc.* **2017**, *139*, 13993−13996.
(41) DuBois, D. L.; Miedaner, A. Mediated electrochemical reduction of CO2. Preparation and comparison of an isoelectronic series of complexes. *J. Am. Chem. Soc.* **1987**, *109*, 113−117.

https://doi.org/10.1021/acscatal.1c01527
ACS Catal. 2021, 11, 8155−8164

(42) DuBois, D. L.; Miedaner, A.; Haltiwanger, R. C. Electrochemical reduction of carbon dioxide catalyzed by [Pd(triphosphine)(solvent)](BF4)2 complexes: synthetic and mechanistic studies. *J. Am. Chem. Soc.* **1991**, *113*, 8753−8764.
(43) Rakowski Dubois, M.; Dubois, D. L. Development of Molecular Electrocatalysts for CO2 Reduction and H2 Production/Oxidation. *Acc. Chem. Res.* **2009**, *42*, 1974−1982.
(44) Therrien, J. A.; Wolf, M. O.; Patrick, B. O. Electrocatalytic Reduction of CO2 with Palladium Bis-N-heterocyclic Carbene Pincer Complexes. *Inorg. Chem.* **2014**, *53*, 12962−12972.
(45) Therrien, J. A.; Wolf, M. O.; Patrick, B. O. Polyannulated Bis(N-heterocyclic carbene)palladium Pincer Complexes for Electrocatalytic CO2 Reduction. *Inorg. Chem.* **2015**, *54*, 11721−11732.
(46) Therrien, J. A.; Wolf, M. O. The Influence of para Substituents in Bis(N-Heterocyclic Carbene) Palladium Pincer Complexes for Electrocatalytic CO2 Reduction. *Inorg. Chem.* **2017**, *56*, 1161−1172.
(47) Therrien, J. A.; Wolf, M. O.; Patrick, B. O. Synthesis and comparison of nickel, palladium, and platinum bis(N-heterocyclic carbene) pincer complexes for electrocatalytic CO2 reduction. *Dalton Trans.* **2018**, *47*, 1827−1840.
(48) Palit, C. M.; Graham, D. J.; Chen, C.-H.; Foxman, B. M.; Ozerov, O. V. Reduction of CO2 to free CO by a Pd(i)−Pd(i) dimer. *Chem. Commun.* **2014**, *50*, 12840−12842.
(49) Boricha, V. P.; Patra, S.; Parihar, S.; Chouhan, Y. S.; Paul, P. Luminescent metalloreceptors with pendant macrocyclic ionophores with NS2O3 donor sites: Synthesis, characterization and ion-binding property. *Polyhedron* **2012**, *43*, 104−113.
(50) Ozutsumi, K.; Kohyama, K.; Ohtsu, K.; Kawashima, T. Thermodynamics of formation of 1,4,7,10,13,16-hexaoxacyclooctadecane (18-crown-6) complexes with calcium, strontium and barium ions in water and dimethylformamide. *J. Chem. Soc., Dalton Trans.* **1995**, *18*, 3081−3085.
(51) Ozutsumi, K.; Ohtsu, K.; Kawashima, T. Thermodynamics of complexation of 18-crown-6 with sodium, potassium, rubidium, caesium and ammonium ions in N,N-dimethylformamide. *J. Chem. Soc., Faraday Trans.* **1994**, *90*, 127−131.
(52) Shannon, R. D. Revised effective ionic radii and systematic studies of interatomic distances in halides and chalcogenides. *Acta Crystallogr., Sect. A* **1976**, *32*, 751−767.
(53) Gokel, G. W. Complexation by Crowns and Cryptands. In *Crown Ethers and Cryptands*; The Royal Society of Chemistry, 1991; Chapter 3, pp 64−98.
(54) Liu, Y.; Han, B.-H.; Inoue, Y.; Ouchi, M. Complexation Thermodynamics of Crown Ethers. 6.1,2 Calorimetric Titration of Cation Complexation with Some Azacrown Ethers. *J. Org. Chem.* **1998**, *63*, 2144−2147.
(55) Cox, R. P.; Sandanayake, S.; Scarborough, D. L. A.; Izgorodina, E. I.; Langford, S. J.; Bell, T. D. M. Investigation of cation binding and sensing by new crown ether core substituted naphthalene diimide systems. *New J. Chem.* **2019**, *43*, 2011−2018.
(56) Mateeva, N.; Deiab, S.; Archibong, E.; Tasheva, D.; Mochona, B.; Gangapuram, M.; Redda, K. Dansyl-substituted aza crown ethers: complexation with alkali, alkaline earth metal cations and ammonium. *Int. J. Chem.* **2011**, *3*, 10−17.
(57) Parham, H.; Shamsipur, M. Spectrophotometric study of some alkali and alkaline earth cryptates in dimethylformamide solution using murexide as a metallochromic indicator. *Polyhedron* **1992**, *11*, 987−991.
(58) Spasyuk, D.; Smith, S.; Gusev, D. G. Replacing Phosphorus with Sulfur for the Efficient Hydrogenation of Esters. *Angew. Chem., Int. Ed.* **2013**, *52*, 2538−2542.
(59) Bai, S.-Q.; Quek, G. Y. H.; Koh, L. L.; Andy Hor, T. S. Crystallographic analysis of different water−halide cluster blends in cationic [(SNS)PdII] pincer complexes. *CrystEngComm* **2010**, *12*, 226−233.
(60) Chantarojsiri, T.; Reath, A. H.; Yang, J. Y. Cationic Charges Leading to an Inverse Free-Energy Relationship for N−N Bond Formation by MnVI Nitrides. *Angew. Chem., Int. Ed.* **2018**, *57*, 14037−14042.
(61) Chantarojsiri, T.; Ziller, J. W.; Yang, J. Y. Incorporation of redox-inactive cations promotes iron catalyzed aerobic C−H oxidation at mild potentials. *Chem. Sci.* **2018**, *9*, 2567−2574.
(62) Kang, K.; Fuller, J.; Reath, A. H.; Ziller, J. W.; Alexandrova, A. N.; Yang, J. Y. Installation of internal electric fields by non-redox active cations in transition metal complexes. *Chem. Sci.* **2019**, *10*, 10135−10142.
(63) Reath, A. H.; Ziller, J. W.; Tsay, C.; Ryan, A. J.; Yang, J. Y. Redox Potential and Electronic Structure Effects of Proximal Nonredox Active Cations in Cobalt Schiff Base Complexes. *Inorg. Chem.* **2017**, *56*, 3713−3718.
(64) Yoo, C.; Dodge, H. M.; Miller, A. J. M. Cation-controlled catalysis with crown ether-containing transition metal complexes. *Chem. Commun.* **2019**, *55*, 5047−5059.
(65) Burns, K. T.; Marks, W. R.; Cheung, P. M.; Seda, T.; Zakharov, L. N.; Gilbertson, J. D. Uncoupled Redox-Inactive Lewis Acids in the Secondary Coordination Sphere Entice Ligand-Based Nitrite Reduction. *Inorg. Chem.* **2018**, *57*, 9601−9610.
(66) Kütt, A.; Movchun, V.; Rodima, T.; Dansauer, T.; Rusanov, E. B.; Leito, I.; Kaljurand, I.; Koppel, J.; Pihl, V.; Koppel, I.; Ovsjannikov, G.; Toom, L.; Mishima, M.; Medebielle, M.; Lork, E.; Röschenthaler, G.-V.; Koppel, I. A.; Kolomeitsev, A. A. Pentakis(trifluoromethyl)-phenyl, a Sterically Crowded and Electron-withdrawing Group: Synthesis and Acidity of Pentakis(trifluoromethyl)benzene, -toluene, -phenol, and -aniline. *J. Org. Chem.* **2008**, *73*, 2607−2620.
(67) Gutmann, V. Solvent effects on the reactivities of organometallic compounds. *Coord. Chem. Rev.* **1976**, *18*, 225−255.
(68) Barlow, J. M.; Yang, J. Y. Thermodynamic Considerations for Optimizing Selective CO2 Reduction by Molecular Catalysts. *ACS Cent. Sci.* **2019**, *5*, 580−588.
(69) Zanello, P. *Inorganic Electrochemistry: Theory, Practice and Application*; The Royal Society of Chemistry: Cambridge, UK, 2003.
(70) Dubois, D. L. Development of Transition Metal Phosphine Complexes as Electrocatalysts for CO2 and CO Reduction. *Comments Inorg. Chem.* **1997**, *19*, 307−325.
(71) Bernatis, P. R.; Miedaner, A.; Haltiwanger, R. C.; DuBois, D. L. Exclusion of Six-Coordinate Intermediates in the Electrochemical Reduction of CO2 Catalyzed by [Pd(triphosphine)(CH3CN)](BF4)-2 Complexes. *Organometallics* **1994**, *13*, 4835−4843.
(72) Herring, A. M.; Steffey, B. D.; Miedaner, A.; Wander, S. A.; DuBois, D. L. Synthesis and Characterization of Water-Soluble [Pd(triphosphine)(CH3CN)](BF4)2 Complexes for CO2 Reduction. *Inorg. Chem.* **1995**, *34*, 1100−1109.
(73) Steffey, B. D.; Miedaner, A.; Maciejewski-Farmer, M. L.; Bernatis, P. R.; Herring, A. M.; Allured, V. S.; Carperos, V.; DuBois, D. L. Synthesis and Characterization of Palladium Complexes Containing Tridentate Ligands with PXP (X = C, N, O, S, As) Donor Sets and Their Evaluation as Electrochemical CO2 Reduction Catalysts. *Organometallics* **1994**, *13*, 4844−4855.
(74) Miedaner, A.; Noll, B. C.; DuBois, D. L. Synthesis and Characterization of Palladium and Nickel Complexes with Positively Charged Triphosphine Ligands and Their Use as Electrochemical CO2-Reduction Catalysts. *Organometallics* **1997**, *16*, 5779−5791.
(75) Wander, S. A.; Miedaner, A.; Noll, B. C.; Barkley, R. M.; DuBois, D. L. Chelate Bite Effects for [Pd(triphosphine)(solvent)]-(BF4)2 Complexes in Electrochemical CO2 Reduction and the Heterolytic Cleavage of Molecular Hydrogen. *Organometallics* **1996**, *15*, 3360−3373.
(76) Bard, A. J.; Faulkner, L. R. *Electrochemical Methods: Fundamentals and Application*, 2nd ed.; John Wiley & Sons, Inc.: Hoboken, NJ, 2001.
(77) Jaworski, J. N.; McCann, S. D.; Guzei, I. A.; Stahl, S. S. Detection of Palladium(I) in Aerobic Oxidation Catalysis. *Angew. Chem., Int. Ed.* **2017**, *56*, 3605−3610.
(78) Putin, A. Y.; Katsman, E. A.; Temkin, O. N.; Bruk, L. G. Complexation equilibria in tetrahydrofuran solutions of palladium(II) and lithium bromides. *Russ. J. Phys. Chem. A* **2017**, *91*, 697−707.
(79) Rosas-Hernández, A.; Steinlechner, C.; Junge, H.; Beller, M. Photo- and Electrochemical Valorization of Carbon Dioxide Using

https://doi.org/10.1021/acscatal.1c01527
ACS Catal. 2021, 11, 8155−8164

Earth-Abundant Molecular Catalysts. *Top. Curr. Chem.* **2017**, *376*, No. 1.
(80) Benson, E. E.; Kubiak, C. P. Structural investigations into the deactivation pathway of the CO2 reduction electrocatalyst Re(bpy)-(CO)3Cl. *Chem. Commun.* **2012**, *48*, 7374−7376.
(81) Finn, C.; Schnittger, S.; Yellowlees, L. J.; Love, J. B. Molecular approaches to the electrochemical reduction of carbon dioxide. *Chem. Commun.* **2012**, *48*, 1392−1399.
(82) Sampson, M. D.; Nguyen, A. D.; Grice, K. A.; Moore, C. E.; Rheingold, A. L.; Kubiak, C. P. Manganese Catalysts with Bulky Bipyridine Ligands for the Electrocatalytic Reduction of Carbon Dioxide: Eliminating Dimerization and Altering Catalysis. *J. Am. Chem. Soc.* **2014**, *136*, 5460−5471.
(83) Smieja, J. M.; Sampson, M. D.; Grice, K. A.; Benson, E. E.; Froehlich, J. D.; Kubiak, C. P. Manganese as a Substitute for Rhenium in CO2 Reduction Catalysts: The Importance of Acids. *Inorg. Chem.* **2013**, *52*, 2484−2491.

https://doi.org/10.1021/acscatal.1c01527
ACS Catal. 2021, 11, 8155−8164